sciendo

Mathematical Modelling in Civil Engineering
Vol. 20-No. 2: 30-36-2025
10.2478/mmce-2025-0009

MODELLING OF STRESS INTO HUMIDIFIED POROUS LAYER UNDER INFLUENCE OF MICROWAVE IRRADIATION

PART III THE NUMERICAL SIMULATION RESULTS

Volodymyr YUZEVYCH - Leading researcher, Professor, D.Sc., Department of Theoretical Principles of Mechanical Desrtructions: Karpenko Phisico-Mechanical Institute of NAS Ukraine,
e-mail: volodymyr.yuzevych@lnu.edu.ua

Taras HOLUBETS – Math of Irst category, M.Sc., Department of Physico-Mechanical Fields:Pidstryhach Institute of Applied Problems of Mechanics and Mathematics of NAS Ukraine, email:taras_holubets@yahoo.com

Abstract: Thus, in the last part of the paper we are demonstrated the numerical results of numerical simulation of mechanical thermodiffusion processes applying to the one-dimensional porous layered sample. So, as conclusion to the previous two parts of the paper: 1. The way of applying the spatial averaging method to the description of the diffusion, electrodynamics and mechanical properties of the porous multiphase composite wetted medium was considered; 2. The set of physical interconnected phenomena in porous wetted materials was defined as the mechanical thermo-diffusion phenomena and the mathematical model was proposed to describe the interconnected moistened, electromagnetic and mechanical fields; 3. On the example of a porous layer the closed system of equations was obtained, which connects the heat and mass transfer processes with an internal microwave heat sources induced by external microwave irradiation and mechanical stresses within the framework of the model of the continuous medium. We are aligned the results of our numerical studies with the characteristic critical time values for the microwave drying and compared the diffusion process into internal and external areas of the porous humidified plate. Also, the mechanical stress state was obtained and analyzed for the porous plate during observer drying period for the small strain values under conditions of absence of external loading.

Keywords: microwave irradiation, porous media, heat and mass transfer, mechanical stress

1. Results and Discussion

Numerical simulation of the stress state of the flat unbounded plate under symmetric microwave irradiation was carried out for the selected porous material: historic ceramic brick. The sorption and capillary properties of the studied material are described into detail in the paper [1], in particular, according to a comparative analysis of semi-empirical models of moisture release or retention, it was established, than at defined averaged porosity $\langle\varphi\rangle = 0.46$ the internal permeability of porous skeleton $k_{\text{in}} = 2.29 \cdot 10^{-13}[m^2]$ and empirical parameter in the model of relative permeabilities for fluid (liquid and gas) phase by van Genuchen [2] $m = 0.67$. Also in the work [2] the relative permeability of liquid k_{rL} and gas k_{rG} phases are defined. It is pointed, that capillary properties of porous material is identically determined by the use of the dimensionless J- Leverett function, which takes a form

$$J(\eta_L) = \left([1/\Theta\,(\eta_L)]^{1/m} - 1\right)^{1-m},$$

here $\Theta = \left(\eta_L - \eta_L^{\text{ir}}\right)/\left(\eta_L^{\text{cr}} - \eta_L^{\text{ir}}\right)$ is the effective pore saturation by liquid, $\eta_L^{\text{ir}} = 0.015$ and $\eta_L^{\text{cr}} = 1$ is the residual and critical pore saturation by liquid for a mentioned material accordingly.

Beginning or equilibrium wetting η_L^{eqv} of porous material is defined by the know [1] relation

$$\eta_L^{\text{eqv}} = \left(\eta_L^{\text{cr}} - \eta_L^{\text{ir}}\right)\Big/\left[1 + \left(\frac{P_{\text{amb}}\sqrt{k_{\text{in}}/\langle\varphi\rangle}}{\sigma(T_{\text{amb}})}\right)^{\frac{1}{1-m}}\right]^{m} + \eta_L^{\text{ir}}, \qquad (1)$$

where $P_{\text{amb}} = 10325[\text{Pa}]$ and $T_{\text{amb}} = 293.15[K]$ are the pressure and temperature of vapor like mixture in surrounding equipment accordingly, and σ is the coefficient of surface tension.

At calculation of matrix elements in the generalized form of heat and mass equation according to known expressions for phase and component flows with following values of molar mass $M_a = 0.029[\text{кmol/kg}]$ for dry air and $M_v = 0.018[\text{кmol/kg}]$ water vapor in two component gas mixture are used. Then the expression for density $\langle\rho_G\rangle^G$ of gas mixture in the approximation of light solution $P_G = p_v/x_v$ has been demonstrated

$$\langle\rho_G\rangle^G = \frac{P_G M_G}{RT} = \frac{M_v+[(1-x_v)/x_v]M_a}{RT} p_v = \langle\rho_v\rangle^G + \langle\rho_a\rangle^G,$$

where $p_v = \phi p_{vs}(T)$ is the partial pressure of unsaturated water vapor, ϕ is the relative humidity of air, p_{vs} is the equilibrium pressure of saturated water vapor, for which value a temperature approximation [3] is satisfied

$$p_{vs}(T) = \text{Exp}\begin{bmatrix} -5800.2206/T + 1.3914993 - 4.8640239\cdot 10^{-2}T + \\ +4.1764768\cdot 10^{-5}T^2 - 1.4452093\cdot 10^{-8}T^3 + \\ +6.5459673\ \text{Ln}(T) \end{bmatrix},$$

here T is the thermodynamic temperature.

Because relative humidity ϕ is defined according to known for investigated material dependence of capillary pressure $p_c(\eta_L, T) = \sigma(T)\sqrt{\langle\varphi\rangle/k_{\text{in}}}J(\eta_L)$ from temperature T and pore saturation η_L by liquid, in such case the equilibrium (initial) value of water vapor molar fraction x_v^{eqv} in wetted porous material is

$$x_v^{\text{eqv}} = \phi_{\text{eqv}} p_{\text{vs}}(T_{\text{amb}})/P_{\text{amb}},$$

where $\phi_{\text{eqv}} = \text{Exp}[-M_v p_c(\eta_L^{\text{eqv}}, T_{\text{amb}})/\langle\rho_L\rangle^L \text{RT}]$ is the initial value of relative humidity, η_L^{eqv} is the corresponding initial equilibrium value of wetting, which has been defined according to relation (1) above.

The effective thermal characteristics of material have been calculated according to known [4] experimental propertied of material, as it is depicted into the Table 1.

Table 1

The thermal properties of phases in the wetted porous material.

Phases	Solid (S)	Liquid (L)	Gas (G)
Thermal conductivity $[Wm^{-1}K^{-1}]$	0.55	0.65	0.025
Thermal capacity $[J\text{kg}^{-1}K^{-1}]$	810	4180	1006

For the defined effective $\bar{\varepsilon}_\omega^{\text{eff}}$ dielectric constant of the investigated wetted poros material, including dielectric loss tangent $\text{tg}\delta_\omega$, numerical calculations were performed in the approximation of the effective medium (EMA) [6] according to relation

$$\sum_\sigma \theta_\sigma \frac{\varepsilon_c^\sigma(\omega) - \bar{\varepsilon}_\omega^{\text{eff}}}{\varepsilon_c^\sigma(\omega) + 2\bar{\varepsilon}_\omega^{\text{eff}}} = 0\ . \qquad (2)$$

The last cubical equation is solved relatively to effective dielectric constant of composite $\bar{\varepsilon}_\omega^{\text{eff}}$, where coefficients are defined by known dimensionless dielectric constant $\varepsilon_c^\sigma(\omega)$ and volume fraction θ_σ of porous media component with usage of experimental data, as it depicted in Table 2.

Table 2

The dielectric constants of porous media components according to EMA approximation (ε_S - solid phase, ε_L- water, ε_G- air).

ν, [Gz]	ε_S		ε_L		ε_G	
	$\varepsilon_S^{'}$	$\varepsilon_S^{''}$	$\varepsilon_L^{'}$	$\varepsilon_L^{''}$	$\varepsilon_G^{'}$	$\varepsilon_G^{''}$

$2.45 \cdot 10^9$	5,86	0,703	80	20	1	0

At this calculation it is taken into account, that density of the solid skeleton $\langle \rho_S \rangle^S = 1500[\text{кг}/m^3]$ and incompressible liquid$\langle \rho_L \rangle^L = 1000[\text{кг}/m^3]$.

The surface tension coefficient σ and the latent heat (enthalpy) of vaporization $\langle r \rangle$ [5] has been reviewed in the form of approximated temperature dependencies

$$\sigma(T) = 0.121978 - 0.0001683T$$

and

$$\langle r \rangle = 2.672 \cdot 10^5 (T - T_{\text{cr1}})^{0.38},$$

where $T_{\text{cr1}} = 647.3[K]$ is the critical temperature (triple point).

The dynamical viscosity of binary gas mixture has been modeled according to the Wilke [8] theory, when for clear components of water vapor μ_v and dry air μ_a it is selected the following [9] numerical approximations

$$\mu_v(T) = 8.85 \cdot 10^{-6} + 3.53 \cdot 10^{-8}(T - T_{\text{cr2}}),$$

$$\mu_a(T) = 17.17 \cdot 10^{-6} + 4.73 \cdot 10^{-8}(T - T_{\text{cr2}}) + 2.22 \cdot 10^{-11}(T - T_{\text{cr2}})^2,$$

here $T_{\text{cr2}} = 273.15[K]$ is the fixed (critical) temperature of water freezing, also

$$\mu_L(T) = 0.6612(T - 229)^{-1.562},$$

where μ_L is the dynamical viscosity approximation according to the work [10] data.

The diffusional properties of components of the vapour-air gas mixture into the pores have been defined with usage of modified by the author paper the diffusion coefficient

$$D_G^{\text{eff}} = \frac{1}{\tau} \frac{\langle \varphi \rangle (1 - \eta_L)}{x_v - \langle \varphi \rangle (1 - \eta_L)(x_v - 1)} D_v^a \quad ,$$

where $D_v^a = 2.29 \cdot 10^{-13}[m/s]$ is the diffusion coefficient of water vapor into the dry air.

2. Conclusions

According to results of heat and mass process numerical simulation the time shift of the near surface wetted and heated zones which are separated by the surfaces S_1 and S_2 is obtained due to the distribution of dimensionless sickness $\Delta h_1/L$ and $\Delta h_2/L$ as it is depicted on the (Fig.1) and (Fig.2) relatively to the surface S_0 of plate symmetry.

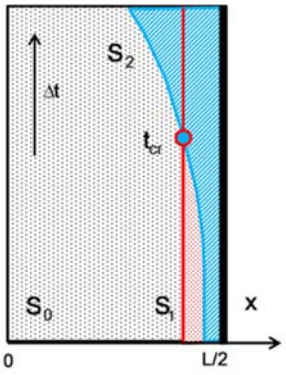

Fig.1 - The evaporation and heating zones moving schema.

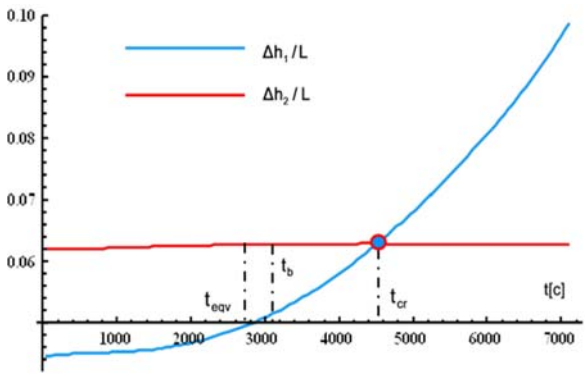

Fig.2 - The evaporation and heating zones moving graph.

Conclusion I: 1. It is exist the fixed critical value of time $t_{\rm cr}$ there is a point of crossover surfaces S_1 and S_2 about that the surface mass transfer coefficient h_m^* (Fig.4) increase non-linearity. It is joined with beginning of processes of intensity liquid evaporation at the near surface wetted zone;

2. It is also established the near linear decreasing of surface heat transfer coefficient h_T^* (Fig.3) along the surface S_1, which is joined with deviation of liquid pore saturation η_L from the averaged equilibrium values at surface of symmetry S_0 of the plate and decreasing of amount of water into near-surface heating zone.

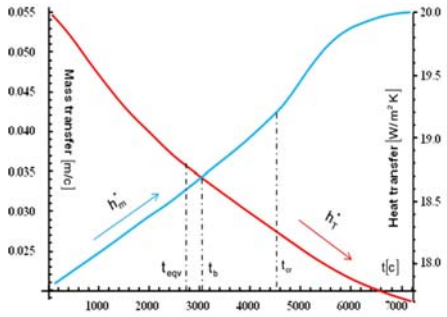

Fig.3 - Surface emission coefficient for heat and mass transfer.

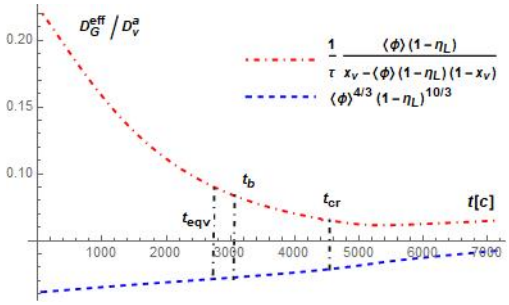

Fig.4 - The internal and surface diffusion coefficients at the evaporation surface.

Conclusion II: 1. In the neighborhood of time value $t_{\rm eqv}$ an equilibrium state of the two component gas mixture of water vapor and dry air follows to a fixed ($x_v = x_a \simeq 1/2$) value, above it the dry air is gradually displaced through the surface S_1 of evaporation and molar fraction of water vapor x_v at the critical point of time $t_{\rm cr}$ follows to a maximum value $x_v = 1$ of saturation; 2. Dimension less diffusivity $D_G^{\rm eff}/D_v^a$ of gas mixture in pores of material for the internal volume of plate and at the evaporation surface are defined in various way, but over time into the region $t \geq t_{\rm cr}$ the calculated values (at $\tau = 4$ as a model tortuosity factor) the both diffusion coefficients on the surface S_1 tends to align.

Solutions of modified system of heat and mass balance for the material of historical ceramic brick are represented in the form of graphical dependencies as it is showing below, here $L^* = n^*\,\Delta L/L_0\,\left(n^* = \Delta L/L_0\right)$ is the dimensionless half thickness of plate.

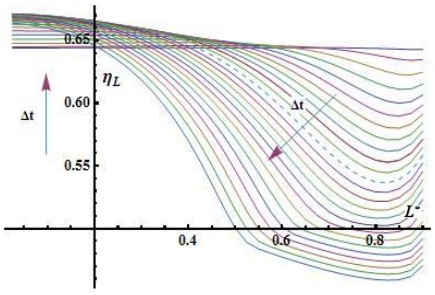

Fig.5 - The distribution of pore saturation by liquid

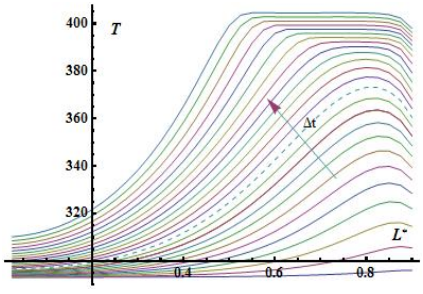

Fig.6 - The distribution of temperature field

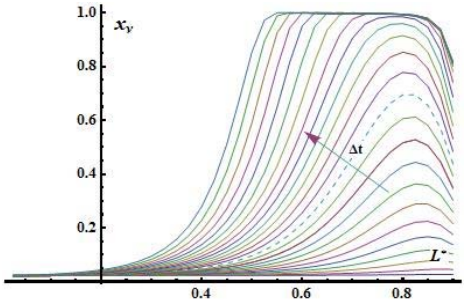

Fig.7 - The distribution of molar fraction for water vapor

Conclusion III: The decreasing of moisture content (see Fig.5) caused by increasing of evaporation sources (see Fig.11 below) that as a result of inhomogeneous microwave heating (Fig.6) of porous plate and change of thermodynamic state (Fig.7) of two component gas mixture.

On the pictures below are shown the distribution of flows by liquid (Fig.8), water vapor (Fig.9) and dry air (Fig.10) along half thickness of plate in the different time intervals.

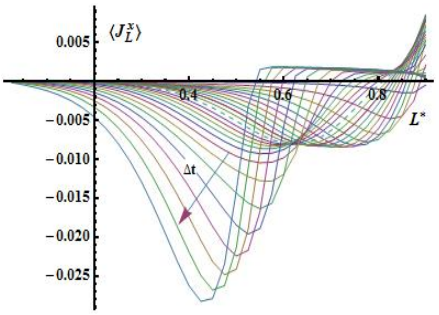

Fig.8 - The distribution of liquid flow

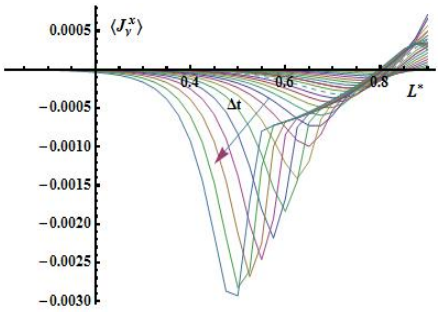

Fig.9 - The distribution of water vapor flow

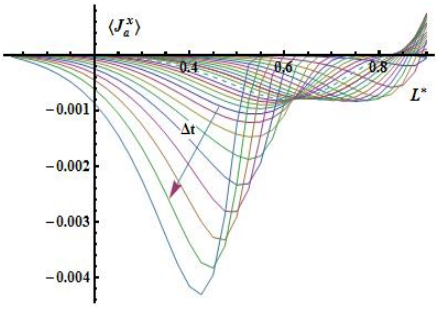

Fig.10 - The distribution of dry air flow

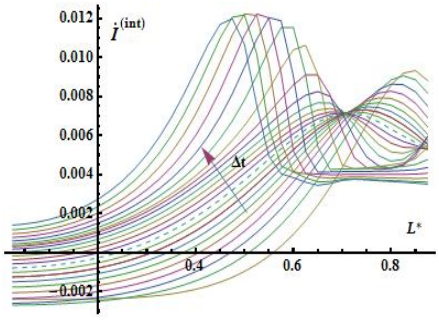

Fig.11 - The distribution of internal evaporation sources

Conclusion IV: In the neighborhood of time point t_b, which corresponds to achievement of boiling temperature at normal conditions (see dashed line, Fig.8-11), it is existing the strong fixed changes of flows distribution for liquid and gas mixture components by the thickness of plate. This is due to the suffice increase into the intensity (Fig. 11) of internal sources of evaporation $\dot{I}^{(\mathrm{int})}$ values along the thickness of the plate into time interval $t > t_b$.

The distribution of specific stresses (Fig. 12) and (Fig. 13) and the small deformations (Fig. 14) and (Fig. 15) into a solid matrix (frame or skeleton) over the half-thickness of the plate is shown by the following graphical dependencies

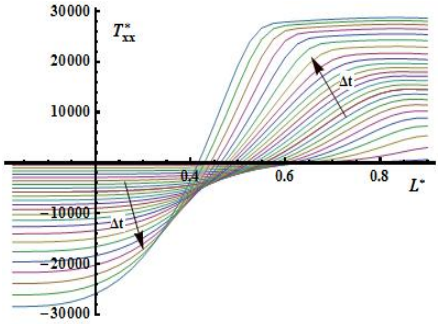

Fig.12 - The distribution of stress in longitudinal direction.

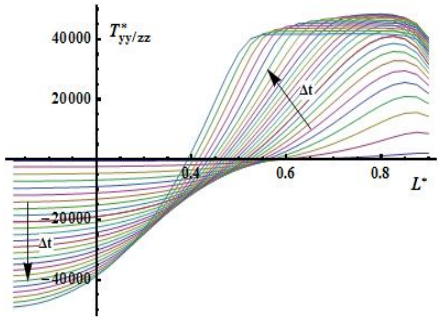

Fig.13 - The distribution of stress in tangential direction.

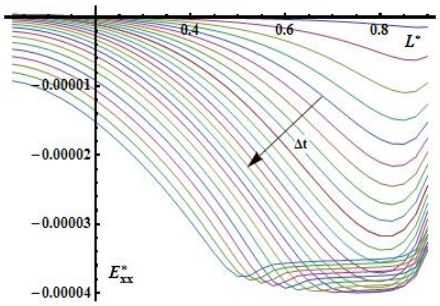

Fig.14 - The distribution of strains in longitudinal direction.

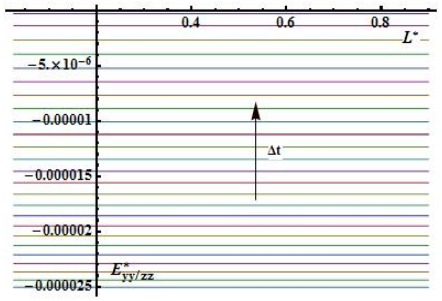

Fig.15 - The distribution of strains in tangential direction.

The dynamics of thermal stress distribution (Fig. 16) along the thickness of the plate is also shown in the form of the corresponding graphical dependence

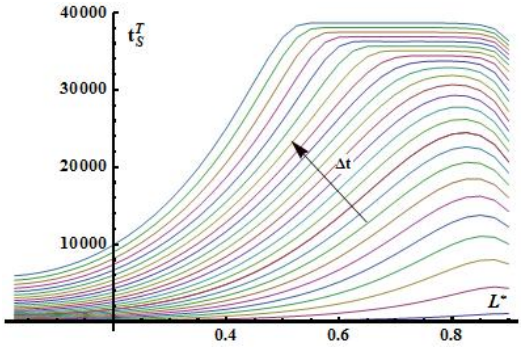

Fig.16 - Distribution of thermal stress in porous skeleton

The distribution of the mechanical stress under the small strain conditions (Fig.14.and Fig.15) for longitudinal direction is strongly correlates (Fig.12) with distribution of temperature filed (Fig.6) during microwave drying. The differences into the form of stress distribution into longitudinal (Fig.12) and tangential directions (Fig.13) are joined with influence of capillary forces due to changes into humidity (fig.5) profiles.

References

[1] Holubets T.V. (2016) Investigation of the structural properties of porous material according to the sorption isotherms and drainage curves. Mathematical modeling and computing,3(1), 23-32. DOI: 10.23939/mmc2016.01.023

[2] van Genuchten M.T. (1980) A Closed-Form Equation for Predicting the Hydraulic Conductivity of Unsaturated Soils. Soil Science Society of America Journal, 44(5), 892–898. DOI:10.2136/sssaj1980.03615995004400050002x.

[3] Kennedy E. ASHRAE-HANDBOOK-Fundamentals (2021) /Chapter 1 Psychrometrics: updates to properties tables and expanded discussion of transport properties of moist air/, https://www.ashrae.org/resources--publications/handbook/2017-ashrae-handbook-fundamentals.

[4] Baggio P., Bonacina C., Grinzato E., Bison P., Bressan C. (1992) Determinazione delle caratteristiche termoigrometriche dei materiali da costruzione porozi, Proc. Congresso Nazionale ATI, Parma, 355-365.

[5] Mayer S.W. (1963) Dependence of surface tension on temperature, The J. of Chem. Phys. 38(8), 1803-1808. DOI: 10.1063/1.1733879

[6] Bruggeman D. A. G. (1935) Ann. Phys., Leipzig, 24, p.636.

[7] Auriault J.L., Lewandowska J. (1996) Diffusion/adsorption/advection macrotransport in soils, Eur. J. Mech – A/Solids, 15(4), 681-704.

[8] Wilke C.R. (1950) A viscosity equation for gas mixtures, The journ. of chem. phys.,.18(4), 517-519. DOI: 10.1063/1.1747673.

[9] Reid R.C., Praunsnitz J.M., Bruce E.P.. The Properties of Gases and Liquids - New-York: MacGraw-Hill, 741p.

[10] Incopera F.P., Dewitt D.P., Bergman T.L., Lavine A.S.. Fundamentals of Heat and Mass Transfer. New-York: J.Wiley&Sons, 1070p.